ELSEVIER

Contents lists available at ScienceDirect

Journal of Colloid and Interface Science

journal homepage: www.elsevier.com/locate/jcis



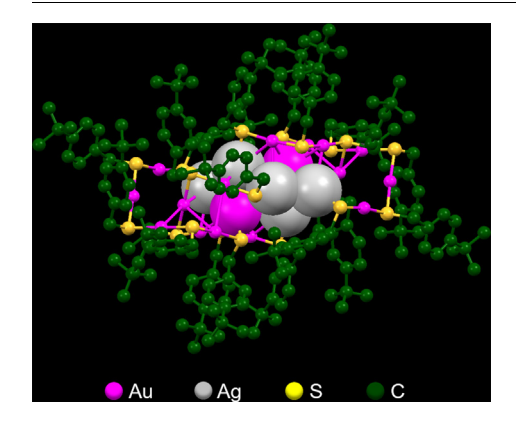
Site-selective substitution of gold atoms in the $Au_{24}(SR)_{20}$ nanocluster by silver



Qi Li ^a, Michael G. Taylor ^b, Kristin Kirschbaum ^c, Kelly J. Lambright ^c, Xiaofan Zhu ^a, Giannis Mpourmpakis ^b, Rongchao lin ^{a,*}

- ^a Department of Chemistry, Carnegie Mellon University, Pittsburgh, PA 15213, USA
- ^b Department of Chemical Engineering, University of Pittsburgh, Pittsburgh, PA 15261, USA
- ^c College of Natural Sciences and Mathematics, University of Toledo, Toledo, OH 43606, USA

G R A P H I C A L A B S T R A C T



ARTICLE INFO

Article history: Received 13 April 2017 Revised 2 June 2017 Accepted 15 June 2017 Available online 16 June 2017

Keywords: Alloy nanoclusters Atomic precision Ligand-exchange

ABSTRACT

The synthesis and structure determination of atomically precise alloy nanoclusters have attracted much attention in recent research. Herein, we report a new alloy nanocluster $\mathrm{Au}_{24\text{--}x}\mathrm{Ag}_x(\mathrm{TBBM})_{20}$ ($x\sim1$) synthesized via a ligand-exchange-induced size/structure transformation method. Its X-ray structure is obtained successfully and the dopant Ag is found to occupy three special positions in the kernel, rather than equivalently over all the kernel sites. This selective occupancy is interesting and DFT calculation results suggest that the relative oxidation state (rationalized as difference in the charge) of the Ag when doped into the cluster is likely determining the most favorable doping positions. This work provides a new strategy for controlled synthesis of new Au-Ag nanoclusters and also reveals a new scenario for the doping position of Ag atoms in Au-Ag bimetal nanoclusters.

© 2017 Elsevier Inc. All rights reserved.

* Corresponding author.

E-mail addresses: li1@andrew.cmu.edu (Q. Li), mgt16@pitt.edu (M.G. Taylor), Kristin.Kirschbaum@utoledo.edu (K. Kirschbaum), kelly.lambright@rockets.utoledo. edu (K.J. Lambright), xz1@andrew.cmu.edu (X. Zhu), gmpourmp@pitt.edu (G. Mpourmpakis), rongchao@andrew.cmu.edu (R. Jin).

1. Introduction

Significant research progress in the synthesis and structure determination and theory of atomically precise ultrasmall gold nanoparticles (also termed as Au nanoclusters) has been achieved in recent years [1–6]. The successes in controlling nanoclusters with atomic precision and further solving their atomic structures by single-crystal X-ray analysis not only offer the opportunity to

fundamentally understand the structure-property relationships, but also make it possible to observe the rich structural transformations between different nanoclusters—which is akin to organic transformation chemistry [7–9]. Such a level of nanochemistry apparently cannot be attained with polydispersed nanoparticles.

Recently, alloy nanoclusters attract much attention in the nanoscience field owing to their controllable and improved properties compared to the homometallic analogues [10-15]. To date, quite a number of gold-based alloy nanoclusters, such as Au₁₅Ag₃, $Au_{24}M_1$ (where M = Pd, Pt), $Au_{36}Pd_2$, $Au_{25-x}Ag_x$, $Au_{38-x}Ag_x$, $[Au_{12+n}Cu_{32}(SR)_{30+n}]^{4-}$, $Au_{36-x}Ag_x$, Au_3Ag_{38} , $Au_{24}Ag_{46}$, have been successfully synthesized by reducing the mixed metal precursors in the presence of thiols [10-25]. In addition to the method of co-reduction of metal salts, metal-exchange is another common method for synthesizing alloy nanoclusters [26–28]. The exchange method involves the first synthesis of nanoclusters of one metal. followed by reaction with a second metal (in the form of salts or metal-thiolate complexes). Recent work by Pradeep and coworkers also reported an intercluster reaction method for obtaining alloy nanoclusters [29]. In the pursuit of alloy nanoclusters, an important goal is to devise new methods for controlling alloy nanoclusters with specific structure. Meanwhile, for the Ag-doped gold nanoclusters, the position of silver dopants varies in different cases [16,22,26], and till now, the determinant factors for the most favorable positions of silver atoms in gold nanoclusters are not clear yet and thus remain to be mapped out.

A ligand-exchange-induced size/structure transformation (LEIST for short) has recently been developed as a new methodology for controlling the size and structure of gold and silver nanoclusters [30-36]. For Au nanoclusters, remarkable examples include the transformations of Au₂₅ to Au₂₈, Au₃₈ to Au₃₆, and Au_{144} to Au_{133} [30–33], and the total structures of the transformed gold nanoclusters have been obtained. The Bakr group has recently also explored this ligand-exchange method in silver nanoclusters [34–36]. Very recently, Zhu and coworkers reported the synthesis and X-ray crystal structure of the Pt₁Ag₂₈(S-Adm)₁₈(PPh₃)₄ nanocluster [37], which was obtained by etching Pt₁Ag₂₄(SPhMe₂)₁₈ simultaneously with Adm-SH (1-adamantanethiol) and PPh₂ ligands. It is of interest whether the LEIST method can also be applied to synthesize new Au-Ag alloy nanoclusters. In addition, mapping out where the dopant silver would go during the transformation would be of major importance.

Herein, we report a new alloy Au-Ag nanocluster formulated as $Au_{24-x}Ag_x(TBBM)_{20}$ ($x\sim 1$), which is transformed from the $[Au_{23-x}Ag_x(c-C_6)_{16}]^-$ ($x\sim 1$, and $c-C_6$ represents cyclohexanethiolate) by reacting with excess $HSCH_2Ph^{-t}Bu$ thiol (abbreviated as TBBM hereafter). Interestingly, the dopant silver is identified to preferentially occupy three special positions of the M_8 (M=mixed Au and Ag) kernel and there is one specific position in the M_8 kernel where no dopant silver can be found. DFT calculation results suggest that the oxidation state of the Ag when doped into the cluster should determine the most favorable doping positions. The optical absorption spectrum of the new $Au_{24-x}Ag_x(TBBM)_{20}$ ($x\sim 1$) is similar to that of its homo gold counterpart $Au_{24}(TBBM)_{20}$, suggesting that the slight silver-doping in the kernel does not severely disturb the electronic structure of the whole cluster.

2. Experimentals

2.1. Chemicals

Tetrachloroauric(III) acid (HAuCl₄·3H₂O, 99.99%, Aldrich), cyclohexanethiol (C₆H₁₁SH, 99%, Aldrich), 4-*tert*-butylbenzylmercaptan (Aldrich), sodium borohydride (NaBH₄, 99.99%, Aldrich), tetraoctylammonium bromide (TOAB) (98%, Fluka), pentane (HPLC grade,

99.9%, Alfa), ethanol (HPLC grade, Aldrich), methanol (HPLC grade, 99%, Aldrich), and dichloromethane (DCM, HPLC grade, 99.9%, Aldrich) were used as received.

2.2. Synthesis and Crystallization of $Au_{24-x}Ag_x(TBBM)_{20}$ $(x \sim 1)$

The $[Au_{23-x}Ag_x(c-C_6)_{16}]^ (x\sim1)$ nanocluster was used as the starting material, which was synthesized by adopting our previously reported method [9]. To obtain the $Au_{24-x}Ag_x(TBBM)_{20}$ $(x\sim1)$ nanocluster, a ligand-exchange reaction with excess TBBM thiol was conducted. In a typical reaction, ~10 mg $[Au_{23-x}Ag_x(c-C_6)_{16}]^-$ clusters were first dissolved in ~2 mL dichloromethane (DCM) and then 2 mL TBBM thiol was added to the reaction. The mixture was stirred for $\sim48-72$ h at room temperature. The resulting nanocluster product was then washed with methanol and ethanol for several times and finally was dissolved in DCM. Single crystal growth of the $Au_{24-x}Ag_x(TBBM)_{20}$ $(x\sim1)$ nanoclusters was performed by diffusion of pentane into the cluster DCM solution for 2–4 days.

2.3. Computational details

Similar to our previous work [9], the Density Functional Theory (DFT) calculations were performed using the BP-86 [38,39] functional combined with the def2-SV(P) basis set [40], accelerated with the resolution of identities (RI) approximation [41,42] as implemented in the Turbomole 6.6 package [43]. Geometry optimizations were carried out using the quasi-Newton-Raphson method without any symmetry constraints. Gibbs free energies were calculated using the harmonic oscillator approach applied to the vibrational modes calculated over the entire nanoparticles at 298.15 K. Charge population analysis was performed via the Natural Bond Orbital analysis method (NBO) [44].

The Au₂₄(SR)₂₀ structure was taken from experimental crystal-lographic information and the R groups of the thiolates were substituted with methyl groups. We note that the BP-86 functional has been successfully utilized on thiolated metal nanocluster systems [45,46] and R = methyl group substitution has had little impact on RS-Au bond strength as has been previously applied in computational NP structural determinations [47–49]. From the optimized Au₂₄(SR)₂₀ cluster, Au atoms were substituted for Ag atoms in each position and the optimized isomers and Gibbs free energies of reaction (see equation below) for Ag doping in different positions are presented in Fig. 5.

$$\text{Au}_{24}(\text{SCH}_3)_{20} + 1/4(\text{Ag}_4(\text{SCH}_3)_4) \rightarrow \text{Au}_{24}\text{Ag}(\text{SCH}_3)_{20} + 1/4(\text{Au}_4(\text{SCH}_3)_4)$$

Tetramers (M_4SR_4) were used as a common reference for the growth and doping reactions for the M^1SR complexes (M = Au or Ag), since these tetramers have been previously shown to be highly thermodynamically stable [50] and similar in structure to the surface "staple motifs" of the clusters. Moreover, these tetramers have been experimentally observed as pre-nucleation species in thiolated group XI bimetallic solutions [51].

3. Results and discussion

The ligand-exchange-induced size/structure transformation from $[Au_{23-x}Ag_x(c-C_6)_{16}]^-$ ($x\sim 1$) to $Au_{24-x}Ag_x(TBBM)_{20}$ ($x\sim 1$) is depicted in Fig. 1, in which both structures are determined by X-ray crystallography. The initial $[Au_{23-x}Ag_x(c-C_6)_{16}]^-$ ($x\sim 1$) cluster possesses a M_{15} (M=Au and Ag), bi-capped cuboctahedron-based kernel, which is protected by two $Au_3(SR)_4$ trimeric staples, two $Au(SR)_2$ monomeric staples, and four bridge (-SR-) ligands. The dopant silver is located at two special positions in the kernel of the $[Au_{23-x}Ag_x(c-C_6)_{16}]^-$ as determined in our previous work [9].

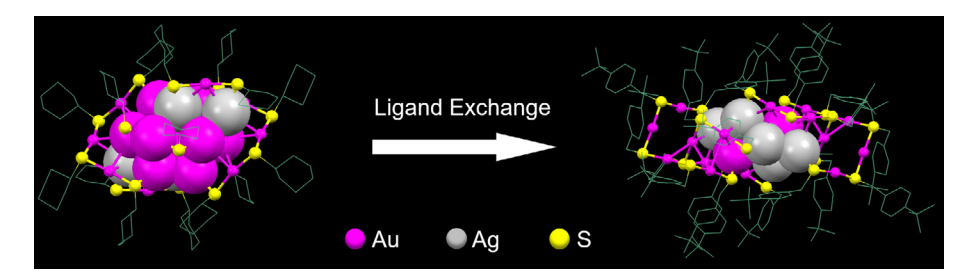


Fig. 1. Ligand-Exchange induced size/structure transformation from $[Au_{23-x}Ag_x(c-C_6)_{16}]^-(x\sim 1)$ to $Au_{24-x}Ag_x(TBBM)_{20}$ ($x\sim 1$) based upon their X-ray structures. Color labels: magenta = Au; grey = Ag partial occupancy site; yellow = S; green = C. Kernel Au and Ag atoms are presented in "spacefill" mode. Surface Au and S atoms are shown in "ball and stick" mode. Carbon tails are shown in wireframe mode. (For interpretation of the references to colour in this figure legend, the reader is referred to the web version of this article.)

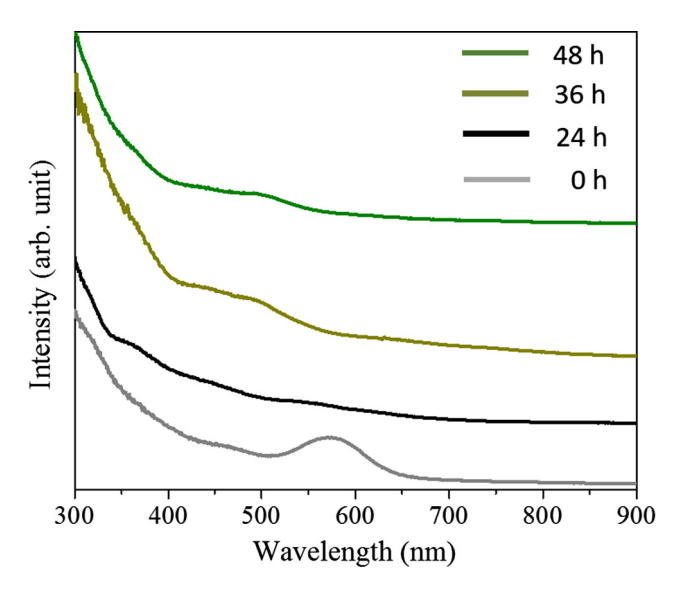


Fig. 2. Evolution of the UV–Vis absorption spectra during the ligand-induced size/structure transformation reaction from $[Au_{23-x}Ag_x(c-C_6)_{16}]^ (x\sim 1)$ to $Au_{24-x}Ag_x(TBBM)_{20}$ $(x\sim 1)$. Note: spectra were taken from the crude product without any purification.

In this work, we employed the LEIST method to synthesize alloy $M_{24}(SR')_{20}$ from its alloy precursor $M_{23}(SR)_{16}^-$ (counterion: tetraoctylammonium, TOA⁺).

The reaction of $[Au_{23-x}Ag_x(c-C_6)_{16}]^-$ with excess TBBM leads to the formation of $Au_{24-x}Ag_x(TBBM)_{20}$. The evolution of UV–Vis absorption during the LEIST reaction is shown in Fig. 2. In the beginning, the starting $[Au_{23-x}Ag_x(c-C_6)_{16}]^-$ ($x\sim 1$) shows an absorption peak at ~ 570 nm (Fig. 2, grey profile). During the first 24 h, the peak at ~ 570 nm disappears and three new absorption shoulders at ~ 360 nm, 450 nm and 550 nm gradually emerge (Fig. 2, black profile). However, in the following 24 h, the spectrum evolves to two shoulder bands at ~ 500 nm and 450 nm. There is no more change in the absorption spectrum for prolonged reaction time. The absorption spectrum of the final product is similar to that of the homogold $Au_{24}(TBBM)_{20}$ reported by our group previously [31], thus, the Au substitution by Ag does not affect the cluster's electronic transitions, at least not at the doping level of $x\sim 1$.

High quality crystals of the final $Au_{24-x}Ag_x(TBBM)_{20}$ product was successfully obtained (Fig. S1) and its atomic structure was revealed by X-ray crystallography (Fig. 3). The structure comprises a bi-tetrahedral, eight-atom Au-Ag kernel (Fig. 3a), which is much smaller than the 15-atom, Au-Ag kernel of the initial $[Au_{23-x}Ag_x(c-C_6)_{16}]^-$ nanocluster. The two partially Ag-doped tetrahedra are anti-prismatically joined together through two triangular faces of the tetrahedra (Fig. 3a), giving rise to a prolate

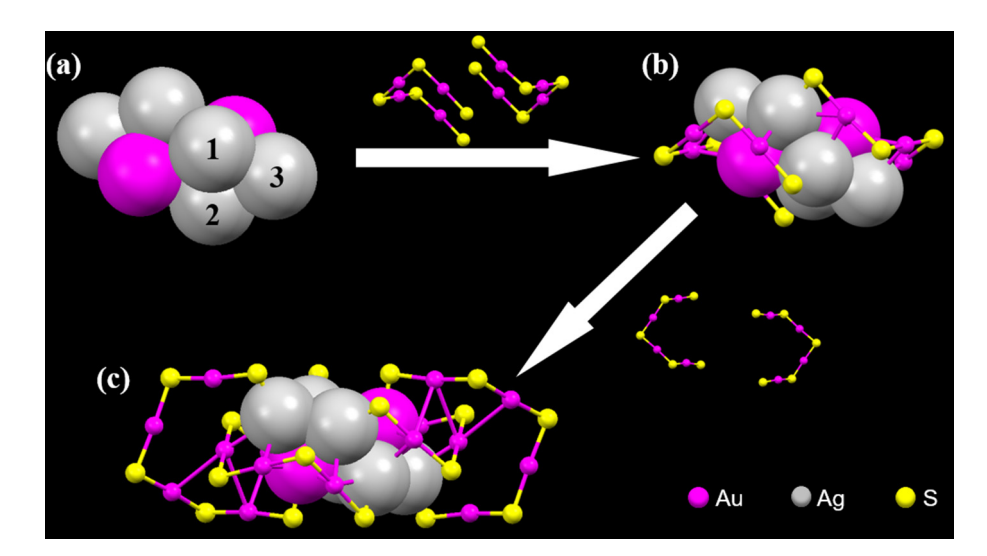


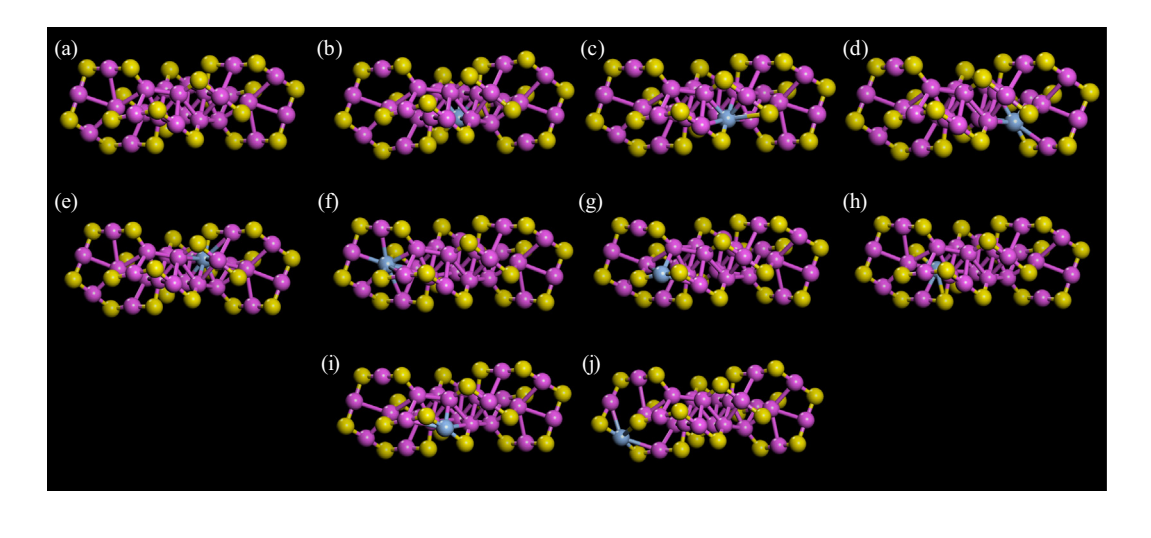
Fig. 3. Anatomy of the structure of $Au_{24-x}Ag_{x}(TBBM)_{20}$ ($x \sim 1$) nanocluster: Starting with the bi-tetrahedral M_8 kernel (a), addition of two tetrameric staple-like motifs, giving rise to (b); followed by the addition of another two tetrameric staples of the same kind, giving rise to $Au_{24-x}Ag_{x}(TBBM)_{20}$ (c). Color labels: magenta = Au; grey = Ag (partial occupancy); yellow = S. (For interpretation of the references to colour in this figure legend, the reader is referred to the web version of this article.)

Table 1Atomic percentages of Au and Ag in the three kernel positions determined by X-ray crystallography. The total percentage of Ag in the entire cluster is one.

	Atomic Site 1	Atomic Site 2	Atomic Site 3
Ag	10%	15%	25%
Au	90%	85%	75%

M₈ structure. The metal-metal bond distances within each individual M₄ tetrahedron range from 2.708(2) Å to 2.766(2) Å (note: the numbers in parentheses are the estimated standard deviations calculated by the refinement program). These bond distances are significantly shorter than that of bulk gold or silver (2.88 Å). On the other hand, the distances of metal-metal bonds at the interface of the two tetrahedra are significantly longer, ranging from 2.954 (2) Å to 3.209(2) Å. Similarly, there are also four tetrameric staples (i.e., $(Au_4(SR)_5)$ protecting the M₈ kernel, each resembles a 'chair' and is reminiscent of the cyclohexane conformation. As shown in Fig. 3b, the Au₄(SR)₅ tetrameric staples are assembled onto the M₈ kernel via bi-dentate bonding (Fig. 3b). The second pair of tetrameric staples rotates by $\sim 90^{\circ}$ relative to the first pair and binds to the exposed faces of the M₈ kernel in a similar manner (Fig. 3c). The dopant Ag can only be found in three special positions of the M₈ kernel. As listed in Table 1, the occupancies of the Au and Ag atom pairs in the kernel are determined to be Au₁/Ag₁: 0.90/0.10 at site 1; Au₂/Ag₂: 0.85/0.15 at site 2; Au₃/Ag₃: 0.75/0.25 at site 3, with the total occupancy of Ag in the entire cluster being one. Interestingly, there is one particular position of the M_8 kernel where no dopant silver can be found. Thus, the composition of $Au_{24-x}Ag_x(TBBM)_{20}$ is $Au_{23}Ag_1(TBBM)_{20}$. The Au/Ag ratio from the crystallographic analysis is also consistent with the elemental analysis (Au:Ag = 22.5:1.5) by energy dispersive X-ray spectroscopy (EDX) under scanning electron microscopy.

The surrounding chemical environments for the four positions in the M₈ kernel are similar as there is only one kind of surface motif, i.e., Au₄(SR)₅, which protects the metal core. It is interesting that the dopant silver is located at three special positions (all being of partial occupancy) in the M₈ kernel of the final Au_{24-x}Ag_x(TBBM)₂₀ product, as opposed to all of the sites in the M₈ kernel. This observation is also different from most previous reports. For example, in the Au_{25-x}Ag_x(SR)₁₈ nanocluster [9,19], the dopant silver is distributed evenly in all the 12 inner shell sites. Also in the Au₁₅Ag₃ case [16], the dopant Ag was found at all the three sites of the middle layer in the core. Why is there one position in the M₈ kernel where no dopant silver can be found? To further verify and rationalize the Ag doping positions within the Au₂₃Ag(TBBM)₂₀ nanocluster framework, DFT calculations were performed. After substituting the TBBM for methyl (CH₃) performing Gibbs free energy analysis on the favorability of doping Ag into various positions within the Au₂₄(SCH₃)₂₀ framework, we have indeed verified that the lowest-energy doping positions correspond to the positions observed in the experiments (see Fig. 4).



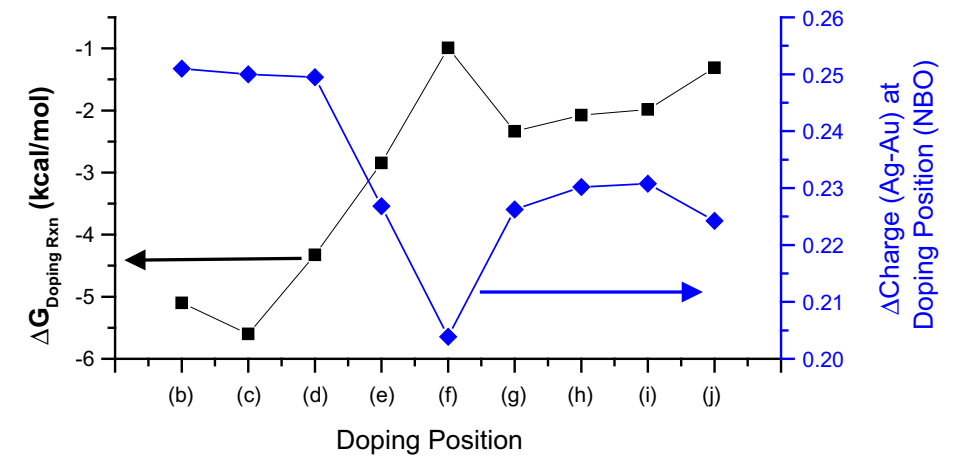


Fig. 4. Upper: (a) $Au_{24}(SCH_3)_{20}$ and (b)-(d) experimental doping positions; (e)-(j) non-experimental dopant positions for Ag atoms tested via DFT in the AgAu₂₃(SCH₃)₂₀ nanoclusters. The -CH₃ groups have been removed for clarity. Lower: Free Energies of doping reactions and ΔCharge (NBO) between Ag atoms in positions of doping (upper) and the equivalent-position Au atoms within the $Au_{24}(SCH_3)_{20}$ nanocluster.

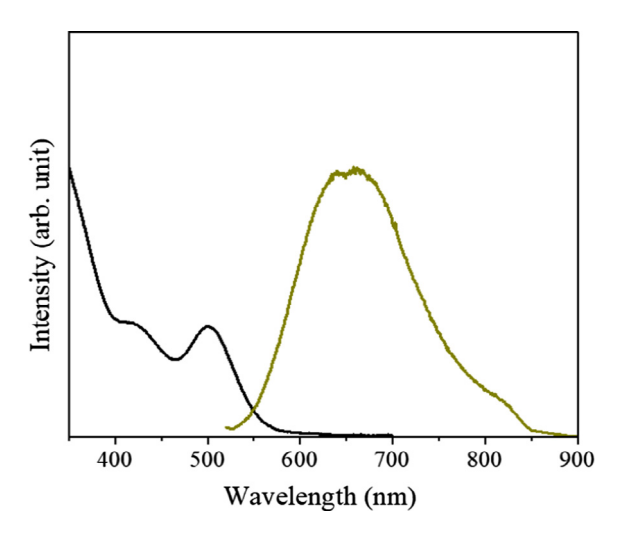


Fig. 5. UV–Vis absorption (black) and PL (grey) spectra of the $Au_{24-x}Ag_x(TBBM)_{20}$ ($x \sim 1$) nanocluster (spectra taken from single crystals re-dissolved in CH_2Cl_2). The PL spectrum was taken under 500 nm excitation.

Upon examining the NBO charges of the Ag atoms when doped in the nanocluster vs the equivalent Au charges within the ${\rm Au}_{24}({\rm SCH}_3)_{20}$ framework, we find that the positions that are lowest in energy impart an identical change in NBO charge on the Ag atoms when doped into the framework. The other doping positions (Fig. 4), however, impose a lower charge state change than the three experimental positions. Therefore, the relative oxidation state of the Ag when doped into the cluster (as indicated by the Δ Charge (Ag-Au) values) is likely determining the most favorable doping positions. Thus, we have explained why the experimental doping positions are observed using DFT and suggest that charge analysis for determining relative oxidation states can potentially aid in screening doping positions into other atomically-precise clusters.

It is important to study whether and how a slight silver-doping influences the overall properties of the gold nanocluster. Among the properties, photoluminescence of metal nanoclusters has attracted wide interest [6,52–54]. The photoluminescence (PL) spectrum of the $Au_{24-x}Ag_x(TBBM)_{20}$ ($x \sim 1$) is shown in Fig. 5, together with the UV-Vis absorption profile. Both spectra were collected from single crystals re-dissolved in dichloromethane (CH₂Cl₂, abbreviated DCM). A distinct absorption peak at 500 nm and a shoulder at ~420 nm can be clearly seen. The PL peak of $Au_{24-x}Ag_x(TBBM)_{20}$ is centered at \sim 670 nm and the quantum yield was determined to be 7%. The PL excitation spectrum was also measured (shown in Fig. S2). From the above results, it can be concluded that the optical absorption of the new Au_{24-x}Ag_x(TBBM)₂₀ $(x \sim 1)$ is similar as its homo gold counterpart, $Au_{24}(TBBM)_{20}$ [31], but the PL maximum shows a \sim 50 nm red-shift. This result suggests that the slight silver-doping ($x \sim 1$) in the kernel does not significantly disturb the ground-state electronic structure (e.g. absorption), but can exert a stronger influence on its excited-state dynamics (e.g. PL) of the whole nanocluster.

4. Conclusion

A new alloy nanocluster, $Au_{24-x}Ag_x(TBBM)_{20}$ ($x\sim 1$), is synthesized from the $[Au_{23-x}Ag_x(c-C_6)_{16}]^-$ ($x\sim 1$) by reaction with excess TBBM thiol. The dopant silver is identified to exclusively occupy three specific positions in the kernel, rather than all the sites of the kernel. DFT calculation results suggest that the relative oxidation state of the Ag when doped into the cluster is likely determining the most favorable doping positions. The optical properties of

the new $\mathrm{Au}_{24\text{--}x}\mathrm{Ag}_x(\mathrm{TBBM})_{20}$ ($x\sim1$) are similar to its homogold counterpart, $\mathrm{Au}_{24}(\mathrm{TBBM})_{20}$, suggesting that the slight silverdoping in the kernel does not disturb the electronic structure of the entire cluster. This work suggests that the ligand-exchange-induced size/structure transformation method can also be applied to the synthesis of alloy Au-Ag nanoclusters, which may largely expand the "library" of the alloy nanoclusters for future development of applications in catalysis [4,55,56], sensing [57], chirality [25,58], optics [59–61] and other fields [6].

Acknowledgements

This work was financial supported by the AFOSR under AFOSR Award No. FA9550-15-1-9999 (FA9550-15-1-0154). GM would like to acknowledge support from the National Science Foundation (CBET-CAREER program) under Grant No. 1652694 and MGT from the National Science Foundation Graduate Research Fellowship under Grant No. 1247842.

Appendix A. Supplementary material

Supplementary data associated with this article can be found, in the online version, at http://dx.doi.org/10.1016/j.jcis.2017.06.049.

References

- [1] C. Zeng, Y. Chen, K. Kirschbaum, K.J. Lambright, R. Jin, Science 354 (2016) 1580–1584.
- [2] T. Higaki, C. Liu, C. Zeng, R. Jin, Y. Chen, N.L. Rosi, R. Jin, Angew. Chem. Int. Ed. 55 (2016) 6694–6697.
- [3] H. Dong, L. Liao, S. Zhuang, C. Yao, J. Chen, S. Tian, M. Zhu, X. Xu, L. Li, Z. Wu, Nanoscale 9 (2017) 3742–3746.
- [4] W.W. Xu, B. Zhu, X.C. Zeng, Y. Gao, Nat. Commun. 7 (2016) 13574.
- [5] P. Maity, S. Xie, M. Yamauchi, T. Tsukuda, Nanoscale 4 (2012) 4027–4037.[6] R. Jin, C. Zeng, M. Zhou, Y. Chen, Chem. Rev. 116 (2016) 10346–10413.
- [7] C. Zeng, Y. Chen, A. Das, R. Jin, J. Phys. Chem. Lett. 6 (2015) 2976–2986.
- [8] Q. Li, S. Wang, K. Kirschbaum, K.J. Lambright, A. Das, R. Jin, Chem. Commun. 52 (2016) 5194–5197.
- [9] Q. Li, T.-Y. Luo, M.G. Taylor, S. Wang, X. Zhu, Y. Song, G. Mpourmpakis, N. Rosi, R. Jin, Sci. Adv. 3 (2017) e1603193.
- [10] Y. Wang, H. Su, C. Xu, G. Li, L. Gell, S. Lin, Z. Tang, H. Häkkinen, N. Zheng, J. Am. Chem. Soc. 137 (2015) 4324–4327.
- [11] S. Wang, X. Meng, A. Das, T. Li, Y. Song, T. Cao, X. Zhu, M. Zhu, R. Jin, Angew. Chem., Int. Ed. 53 (2014) 2376.
- [12] G. Soldan, M.A. Aljuhani, M.S. Bootharaju, L.G. AbdulHalim, M.R. Parida, A.H. Emwas, O.F. Mohammed, O.M. Bakr, Angew. Chem. Int. Ed. 55 (2016) 5749–5752
- [13] J.L. Zeng, Z.J. Guan, Y. Du, Z.A. Nang, Y.M. Lin, Q.M. Wang, J. Am. Chem. Soc. 138 (2016) 7848–7851.
- [14] M.S. Bootharaju, C.P. Joshi, M.R. Parida, O.F. Mohammed, O.M. Bakr, Angew. Chem. Int. Ed. 55 (2016) 922–926.
- [15] H. Qian, D.-E. Jiang, G. Li, C. Gayathri, A. Das, R.R. Gil, R. Jin, J. Am. Chem. Soc. 134 (2012) 16159–16162.
- [16] J. Xiang, P. Li, Y. Song, X. Liu, H. Chong, S. Jin, Y. Pei, X. Yuan, M. Zhu, Nanoscale 7 (2015) 18278–18283.
- [17] Y. Negishi, T. Iwai, M. Ide, Chem. Commun. 46 (2010) 4713-4715.
- [18] Y. Negishi, K. Igarashi, K. Munakata, W. Ohgake, K. Nobusada, Chem. Commun. 48 (2012) 660–662.
- [19] C. Kumara, C.M. Aikens, A. Dass, J. Phys. Chem. Lett. 5 (2014) 461-466.
- [20] S. Yamazoe, W. Kurashige, K. Nobusada, Y. Negishi, T. Tsukuda, J. Phys. Chem. C 118 (2014) 25284–25290.
- [21] J. Yan, H. Su, H. Yang, S. Malola, S. Lin, H. Häkkinen, N. Zheng, J. Am. Chem. Soc. 137 (2015) 11880–11883.
- [22] J. Fan, Y. Song, J. Chai, S. Yang, T. Chen, B. Rao, H. Yu, M. Zhu, Nanoscale 8 (2016) 15317–15322.
 [23] Z. Wang, R. Senanayake, C.M. Aikens, W.-M. Chen, C.-H. Tung, D. Sun,
- Nanoscale 8 (2016) 18905–18911.
- [24] S. Wang, S. Jin, S. Yang, S. Chen, Y. Song, J. Zhang, M. Zhu, Sci. Adv. 1 (2015) e1500441.
- [25] H. Yao, R. Kobayashi, J. Colloid Interface Sci. 419 (2014) 1–8.
- [26] S. Wang, Y. Song, S. Jin, X. Liu, J. Zhang, Y. Pei, X. Meng, M. Chen, P. Li, M.J. Zhu, J. Am. Chem. Soc. 137 (2015) 4018–4021.
- [27] Z. Wu, Angew. Chem., Int. Ed. 51 (2012) 2934–2938.
- [28] L. Liao, S. Zhou, Y. Dai, L. Liu, C. Yao, C. Fu, J. Yang, Z. Wu, J. Am. Chem. Soc. 137 (2015) 9511–9514.
- [29] K.R. Krishnadas, A. Ghosh, A. Baksi, I. Chakraborty, G. Natarajan, T. Pradeep, J. Am. Chem. Soc. 138 (2016) 140–148.

- [30] C. Zeng, H. Qian, T. Li, G. Li, N.L. Rosi, B. Yoon, R.N. Barnett, R.L. Whetten, U. Landman, Angew. Chem., Int. Ed. 51 (2012) 13114–13118.
- [31] A. Das, T. Li, G. Li, K. Nobusada, C. Zeng, N.L. Rosi, R. Jin, Nanoscale 6 (2014) 6458–6462.
- [32] C. Zeng, Y. Chen, K. Kirschbaum, K. Appavoo, M.Y. Sfeir, Sci. Adv. 1 (2015) e1500045.
- [33] C. Zeng, T. Li, A. Das, N.L. Rosi, R. Jin, J. Am. Chem. Soc. 135 (2013) 10011–10013.
- [34] M.S. Bootharaju, V.M. Burlakov, T.M.D. Besong, C.P. Joshi, L.G. AbdulHalim, D. M. Black, R.L. Whetten, A. Goriely, O.M. Bakr, Chem. Mater. 27 (2015) 4289–4297.
- [35] M.S. Bootharaju, C.P. Joshi, L.G. AbdulHalim, J.A. Mohammad, O.M. Bakr, Chem. Mater. 28 (2016) 3292–3297.
- [36] L.G. AbdulHalim, N. Kothalawala, L. Sinatra, A. Dass, O.M. Bakr, J. Am. Chem. Soc. 136 (2014) 15865–15868.
- [37] X. Kang, M. Zhou, S. Wang, S. Jin, G. Sun, M. Zhu, R. Jin, Chem. Sci. (2017), http://dx.doi.org/10.1039/C6SC05104A.
- [38] A.D. Becke, Phys. Rev. A 38 (6) (1988) 3098–3100.
- [39] J.P. Perdew, Phys. Rev. B 33 (12) (1986) 8822-8824.
- [40] F. Weigend, M. Häser, H. Patzelt, R. Ahlrichs, Chem. Phys. Lett. 294 (1998) 143–152.
- [41] F. Weigend, M. Häser, Theor. Chem. Acc. 97 (1997) 331.
- [42] M. Feyereisen, G. Fitzgerald, A. Komornicki, Chem. Phys. Lett. 208 (1993) 359–363
- [43] R. Ahlrichs, M. Bär, M. Häser, H. Horn, C. Kölmel, M. Bar, M. Haser, H. Horn, C. Kolmel, Chem. Phys. Lett. 162 (1989) 165–169.
- [44] A.E. Reed, R.B. Weinstock, F.J. Weinhold, Chem. Phys. 83 (1985) 735.
- [45] A.P. Scott, L.J. Radom, Phys. Chem. 100 (1996) 16502-16513.

- [46] A. Fernando, C.M. Aikens, J. Phys. Chem. C 119 (2015) 20179–20187.
- [47] B.M. Barngrover, C.M. Aikens, J. Phys. Chem. A 117 (2013) 5377-5384.
- [48] Y. Pei, Y. Gao, X.C. Zeng, J. Am. Chem. Soc. 130 (2008) 7830–7832.
- [49] H. Grönbeck, H. Häkkinen, R.L. Whetten, J. Phys. Chem. C 111 (2008) 15940– 15942.
- [50] G. Mpourmpakis, S. Caratzoulas, D.G. Vlachos, Nano Lett. 10 (2010) 3408–3413.
- [51] L.E. Marbella, D.M. Chevrier, P.D. Tancini, O. Shobayo, A.M. Smith, K.A. Johnston, C.M. Andolina, P. Zhang, G. Mpourmpakis, J.E. Millstone, J. Am. Chem. Soc. 137 (2015) 15852–15858.
- [52] X. Yuan, X.Y. Dou, K.Y. Zheng, J.P. Xie, Part. Part. Syst. Charact. 32 (2015) 613–629.
- [53] B. Santiago-Gonzalez, C. Vazquez-Vazquez, M.C. Blanco-Varela, JMG. Martinho, J.M. Ramallo-Lopez, F.G. Requejo, M.A. Lopez-Quintela, J. Colloid Interface Sci. 455 (2015) 154–162.
- [54] C. Wang, L. Xu, X. Xu, H. Cheng, H. Sun, Q. Lin, C. Zhang, J. Colloid Interface Sci. 416 (2014) 274–279.
- [55] Q. Li, A. Das, S. Wang, Y. Chen, R. Jin, Chem. Commun. 52 (2016) 14298–14301.
- [56] C. Lavenn, F. Albrieux, A. Tuel, A. Demessence, J. Colloid Interface Sci. 418 (2014) 234–239.
- [57] A. Ghosh, V. Jeseentharani, M.A. Ganayee, R.G. Hemalatha, K. Chaudhari, C. Vijayan, T. Pradeep, Anal. Chem. 86 (2014) 10996–11001.
- [58] A. Sels, N. Barrabes, S. Knoppe, T. Burgi, Nanoscale 8 (2016) 11130–11135.
- [59] A. Tlahuice-Flores, Prog. Nat. Sci.-Mater. Int. 26 (2016) 510–515.
- [60] A. Fortunelli, M. Stener, Prog. Nat. Sci.-Mater. Int. 26 (2016) 467-476.
- [61] I. Russier-Antoine, F. Bertorelle, R. Hamouda, D. Rayane, P. Dugourd, Z. Sanader, V. Bonacic-Koutecky, P.F. Brevet, R. Antoine, Nanoscale 8 (2016) 2892–2898.